Palaeogeography, Palaeoclimatology, Palaeoecology 576 (2021) 110487

Contents lists available at ScienceDirect

Palaeogeography, Palaeoclimatology, Palaeoecology

journal homepage: www.elsevier.com/locate/palaeo

High-precision U-Pb zircon geochronology of the Miocene Bisciaro Formation, Contessa Section, Italy: A case study for requisite radioisotopic calibration of bio- and magnetostratigraphy

Jennifer Kasbohm [a,*,1], Blair Schoene [a], Alessandro Montanari [b], Rodolfo Coccioni [c]

[a] Department of Geosciences, Princeton University, Princeton, NJ 08544, United States of America
[b] Osservatorio Geologico di Coldigioco, Cda. Coldigioco 4, 62021 Apiro, Italy
[c] Università degli Studi di Urbino "Carlo Bo", 61029 Urbino, Italy

ARTICLE INFO

Editor: Thomas Algeo

Keywords:
Burdigalian
Global Stratotype Section and Point
Umbria-Marche basin
Planktonic foraminifera
Paleomagnetism
Volcaniclastics

ABSTRACT

The stratigraphic sections along the Contessa Valley near Gubbio, Italy, have yielded numerous insights into Late Mesozoic and Cenozoic Earth history from integrated biostratigraphic, magnetostratigraphic, and chemostratigraphic studies of the carbonates comprising the sections. However, the quality of microfossil preservation, faithfulness of magnetic mineralogy, and presence of hiatuses may hinder the development of accurate and precise age models for the critical climatic events documented by these rocks. The deposition of volcaniclastic horizons containing zircon in the uppermost, Miocene portion of the section allows for the acquisition of absolute, high-precision ages through U-Pb zircon geochronology. Here, we present four U-Pb ages from the Bisciaro Formation in the Contessa – Il Testimone section, which revise prior $^{40}Ar/^{39}Ar$ geochronology that was less precise and potentially affected by alteration. We find that the section was deposited between ~22.3 and 20.1 Ma, with a hiatus lasting ~1 Myr in the Lower Bisciaro. Our results suggest that biostratigraphic data may be skewed by an underestimation of the true stratigraphic range of foraminifera, as a result of poor preservation, and that prior magnetostratigraphy overestimated the number of magnetic field reversals. Given these inconsistencies and the presence of hiatuses in the section, we reject the recent suggestion that the Contessa section could serve as the Burdigalian Global Stratigraphic Section and Point (GSSP). We suggest that wherever possible, absolute geochronology should be used to calibrate sedimentary sections, especially candidate GSSPs, as a way to verify the accuracy of age models based on biostratigraphy, magnetostratigraphy, and astronomical tuning.

1. Introduction

Earth's climate history is archived in carbonate sediments, and thus ascertaining the tempo of climatic change depends on constructing reliable age models for carbonate successions. The Contessa Valley near Gubbio (central Italy) is noteworthy for its nearly continuous sedimentary record of Late Mesozoic and Cenozoic Earth history. Spanning the base of the Cretaceous to the Middle Miocene (Alvarez, 2019, and references therein), the stratigraphic sections in the Contessa Valley contain the 'Selli' and 'Bonarelli' black shales from which the Cretaceous Oceanic Anoxic Events were inferred, the Cretaceous-Paleogene boundary clay with the iridium anomaly that led to the impact hypothesis for the Cretaceous-Paleogene extinction (Alvarez et al., 1980), hyperthermal events in the Early Paleogene and Middle Eocene, and sedimentary evidence for intervals of tectonic activity in the Mediterranean (Montanari et al., 1997). Numerous bio-, chemo-, and magnetostratigraphic studies have been performed to construct age models for these sections (Coccioni et al., 2010; Jovane et al., 2007), many calibrated in age by astronomical tuning (Galeotti et al., 2010; Jovane et al., 2010).

The Lower Miocene Bisciaro Formation, near the top of the Contessa section, is noteworthy for its quantity of volcaniclastic layers that are interbedded with marly and glauconitic limestone. This unit is interpreted as representing the transition from pelagic carbonate deposition to siliciclastic turbidite deposition in the Apennine foredeep, concurrent with a pulse of calc-alkaline intermediate volcanism elsewhere in the

* Corresponding author.
E-mail addresses: jennifer.kasbohm@yale.edu (J. Kasbohm), bschoene@princeton.edu (B. Schoene), sandro.coldigioco@gmail.com (A. Montanari), rodolfo.coccioni@uniurb.it (R. Coccioni).
[1] Present address: Department of Earth & Planetary Sciences, Yale University, New Haven, CT 06510.

https://doi.org/10.1016/j.palaeo.2021.110487
Received 27 January 2021; Received in revised form 17 May 2021; Accepted 19 May 2021
Available online 25 May 2021

Mediterranean (Guerrera et al., 2015; Montanari et al., 1997). Because the volcaniclastic layers contained biotite and plagioclase suitable for dating through $^{40}Ar/^{39}Ar$ geochronology, the Bisciaro was included in an integrated study of the Lower Miocene Contessa-Il Testimone (CT) portion of section (43.38248°N, 12.56324°E, 600 m; Fig. 1) that combined $^{40}Ar/^{39}Ar$ geochronology, biostratigraphy, chemostratigraphy, and magnetostratigraphy (Montanari et al., 1997; Montanari et al., 1991). Astronomical tuning has not been successfully performed in the CT section because there are documented hiatuses. However, the presence of bentonitic layers and advances in radioisotopic dating encourage an updated calibration of magnetostratigraphic and biostratigraphic data produced from this 21-m-thick section, especially since prior integrated stratigraphy in the CT section still informs ages of biostratigraphic data reported in the latest Geologic Time Scale (GTS 2020) (Raffi et al., 2020).

Prior $^{40}Ar/^{39}Ar$ geochronology from the CT section yielded ages of 21.88 ± 0.32 Ma and 19.67 ± 0.30 Ma through incremental heating of plagioclase separates. Paleomagnetic and biostratigraphic study suggested that nearly 5 Myr were represented in the CT and overlying CV sections, from ~22.5–17.5 Ma (Montanari et al., 1997). Here, we use high-precision U-Pb CA-ID-TIMS geochronology to produce four new ages on volcaniclastic horizons from the CT section. This technique has been similarly crucial in numerically calibrating biostratigraphic age models throughout the Phanerozoic (e.g., Davydov et al., 2012; Day

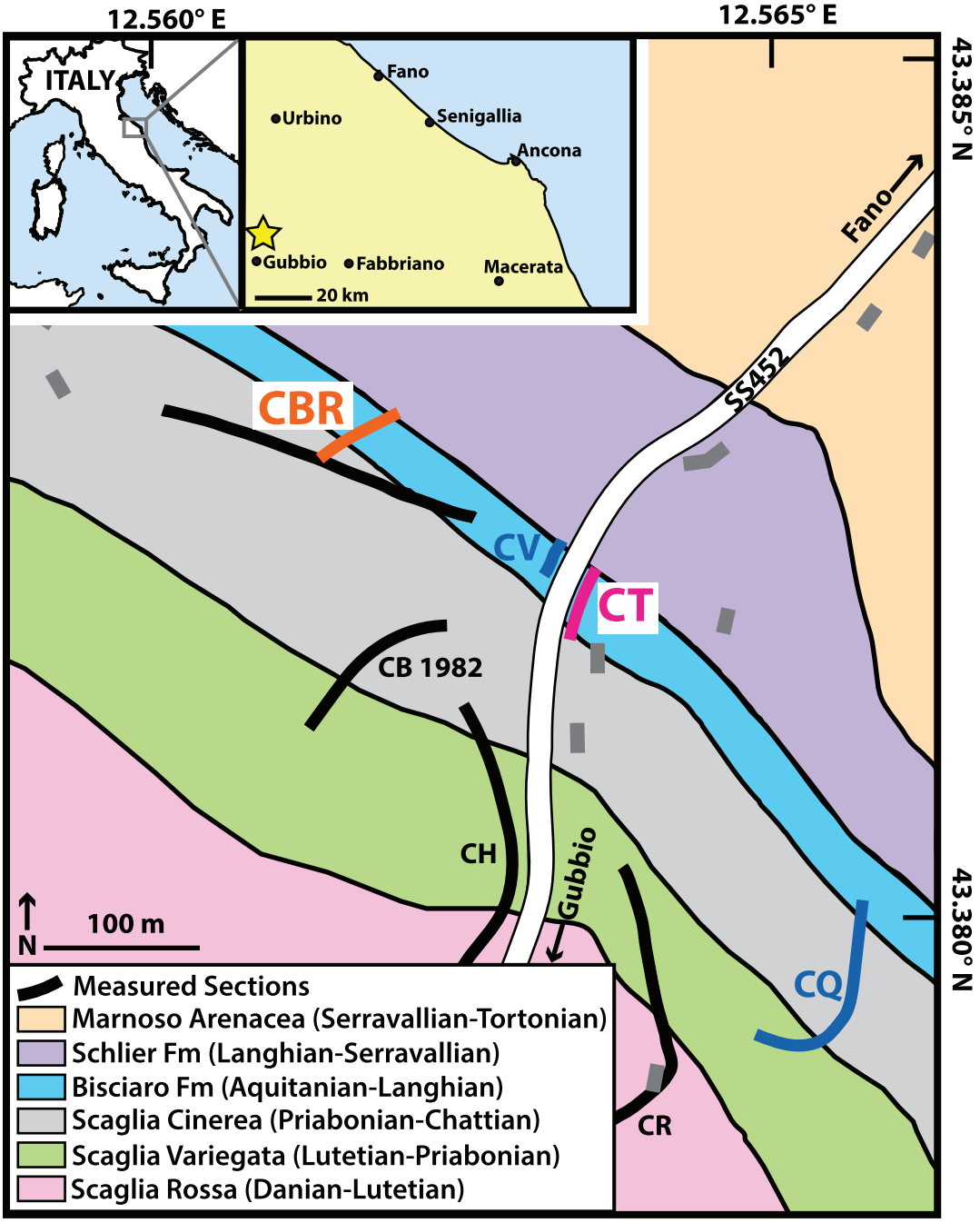

Fig. 1. Geologic map of the Contessa Valley. Regional geographic and geologic context of measured sections in the Contessa Valley, after Coccioni et al. (2008). Star indicates location of geologic map. CT – Contessa-Il Testimone (subject of this study); CBR – Contessa Barbetti Road (orange line indicates position of measured section of Fabbrini et al., 2019); CQ – Contessa Quarry; CV – Contessa Valderchia; CB – Contessa Barbetti; CH – Contessa Highway; CR – Contessa Road.

et al., 2015; Schoene et al., 2010). We show that this section represents only 2 Myr of deposition, including an ~1 Myr hiatus. We suggest that the biostratigraphic and paleomagnetic data obtained for this carbonate section may be unreliable, as a result of poor foraminiferal preservation and magnetic mineralogy. Even with our new high-precision geochronology, we reject the recent suggestion of Fabbrini et al. (2019) that the Aquitanian-Burdigalian GSSP (Global Stratotype Section and Point) be placed in the Contessa section, because of these numerous inconsistencies when integrated stratigraphy is attempted.

2. Geologic setting

The sediments of the Umbria-Marche basin were deposited on Hercynian (Variscan) continental crust, on the northern margin of the African Plate. Beginning ~200 Ma, extensional tectonics led to progressive rifting, and the development of a passive margin that experienced deepening from a shallow-water to pelagic environment from the Jurassic to Early Miocene. Carbonates were deposited during this interval, with a gradual increase in fine siliciclastic content leading to marly units (Guerrera et al., 2015). The Scaglia Bianca, Scaglia Rossa, and Scaglia Variegata Formations (Fig. 1) consist of hard limestones with varying contributions of chert and marl deposited through the Cretaceous, Paleocene, and most of the Eocene (Alvarez, 2019). The Scaglia Cinerea comprises 100 m of homogeneous blue-grey, biomicritic, well-bedded marly limestones that were deposited in a deep-water pelagic basin from the late Eocene through the Oligocene (Montanari et al., 1997). The Lower Miocene Bisciaro Formation, composed of hard pelagic marly limestones, pelagic calcareous marls, and glauconitic-sandy limestones, marks a peak in volcaniclastic contribution, which continued to a lesser extent during the deposition of the overlying Schlier Formation soft marls and alternating siliceous-calcareous marly limestones (Deino et al., 1997). The Langhian Marnoso Arenacea Formation marks the Middle-Upper Miocene transition to siliciclastic turbiditic deposition in the Apennine foredeep in the Contessa Valley (Montanari et al., 1997).

3. Methods

Geochronology samples were collected from the CT section in September 2018 (Figs. 1 and 2). The geochronology methods below are as described in Kasbohm and Schoene (2018), Schoene et al. (2015) and Samperton et al. (2015).

3.1. Zircon separation and preparation

Zircons were separated from their host rock through standard methods of crushing, gravimetric-, and magnetic-separation techniques using a blender, shatterbox, hand pan, hand magnet, Frantz isodynamic separator, and methylene iodide. Zircons from the least magnetic and most dense mineral separate were transferred in bulk to quartz crucibles and annealed in a muffle furnace at 900 °C for 48 h after Mattinson (2005). After annealing, 20–40 zircon grains from each sample were photographed (Fig. S1) and picked in reagent-grade ethanol for analysis. Given the low radiogenic Pb content of the samples,

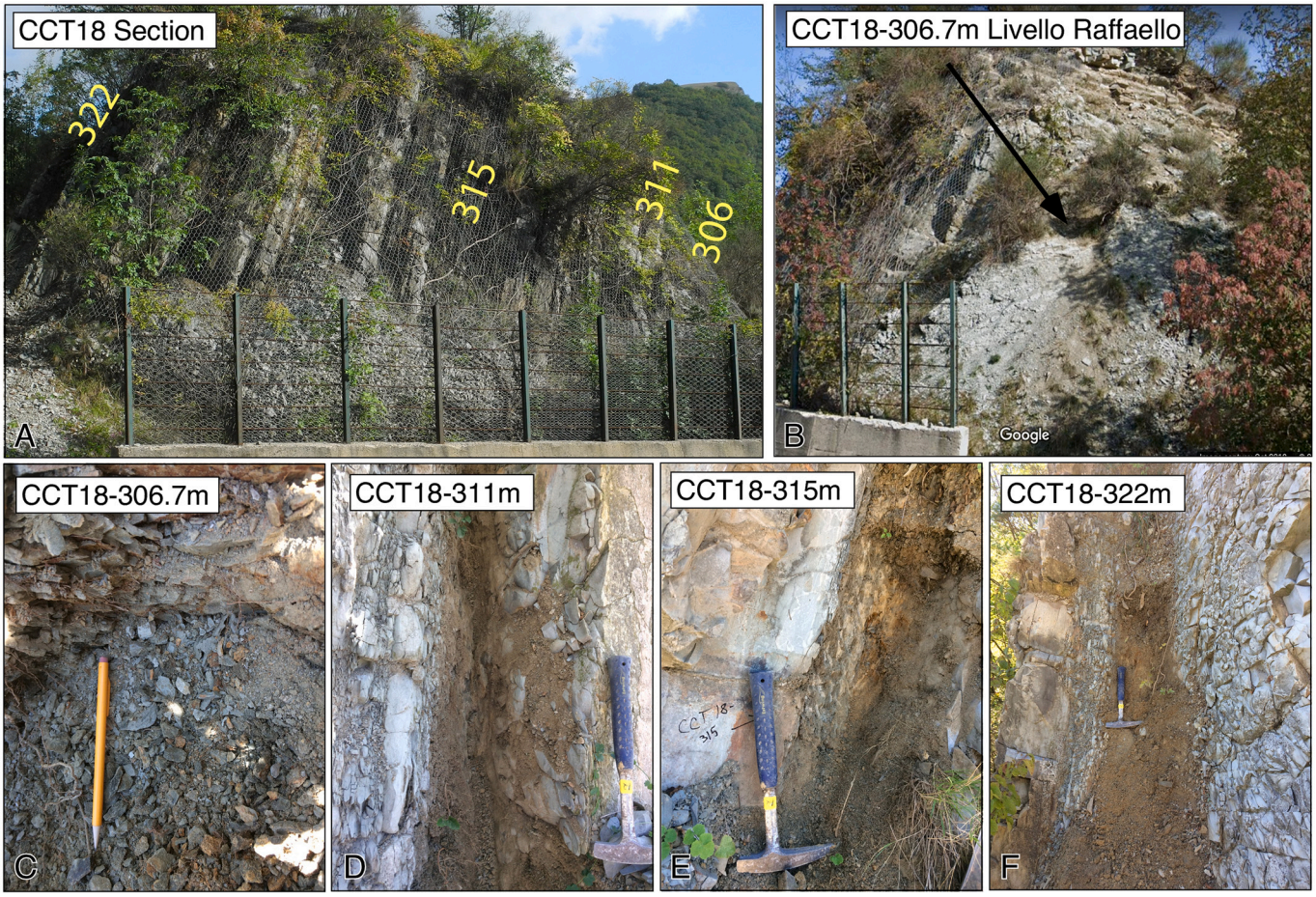

Fig. 2. The Contessa Testimone section. A) Panoramic view of the section as it appeared in 2018 with the position of sampled meter levels relocated from Montanari et al. (1991); B) Location of the Livello Raffaello bentonite marking the base of the Bisciaro Formation; C) Close up photo of the Livello Raffaello; D) Close up photo of the volcaniclastic layer at 311 m; E) Close up photo of the volcaniclastic layer at 315 m; F) Close up photo of the volcaniclastic layer at 322 m.

cathodoluminescence images were not obtained. Euhedral grains with a range of morphologies were selected, while those with visible cracks, inclusions, and cores were avoided. Individual grains were transferred using stainless steel picking tools to separate 3-mL Savillex Hex beakers containing distilled acetone and taken to the clean lab for analysis.

3.2. U-Pb zircon ID-TIMS analysis

Single zircon grains were loaded into 200 uL Savillex "micro"-capsules with 100 μL 29 M HF + 15 μL 3 N HNO_3 for a single leaching step in high-pressure Parr bombs at 185 °C for 12 h to remove crystal domains affected by Pb loss (Mattinson, 2005). Grains were rinsed post-leaching in 6 N HCl, MQ H_2O, 3 N HNO_3, and 29 M HF prior to spiking with EARTHTIME ^{205}Pb-^{233}U-^{235}U tracer and addition of 100uL 29 M HF + 15 μL 3 N HNO_3 (Condon et al., 2015; McLean et al., 2015). Zircons were then dissolved to completion in Parr bombs at 210 °C for 48 h. Dissolved zircon solutions were subsequently dried down, dissolved in 100 μL 6 N HCl, and converted to chlorides in Parr bombs at 185 °C for 12 h, after which solutions were dried again and brought up in 50 μL 3 N HCl. The U-Pb and trace element aliquots were then separated by anion exchange chromatography using 50 μL columns and AG-1 × 8 resin (200–400 mesh, chloride from Eichrom) (Krogh, 1973), and dried down with a microdrop of 0.015 M H_3PO_4. The dried U and Pb aliquot was loaded in a silica gel emitter (Gerstenberger and Haase, 1997) to an outgassed zone-refined Re filament.

Isotopic determinations were performed using an IsotopX PhoeniX-62 thermal ionization mass spectrometer (TIMS) at Princeton University, with Pb analysis performed in peak-hopping mode on a Daly-photomultiplier ion-counting detector. A correction for mass-dependent Pb fractionation was applied using a Pb fractionation of 0.182 ± 0.041%/amu (2σ), as determined by repeat measurements of NBS982 at Princeton. A Daly-photomultiplier deadtime of 28.8 ns was used, as determined by repeat measurements of NBS standards. Corrections for interfering isotopes under masses 202, 204, and 205 were made cycle-by-cycle by measuring masses 201 and 203 and assuming they represent $^{201}BaPO_4$ and ^{203}Tl and using natural isotopic abundances to correct for $^{202}BaPO_4$, $^{204}BaPO_4$, $^{205}BaPO_4$, and ^{205}Tl.

UO_2 measurements were performed in static mode on Faraday cups with a bulk U fractionation correction calculated from the deviation of measured $^{233}U/^{235}U$ from the known tracer $^{233}U/^{235}U$ (0.995062 ± 0.000054 (1σ)), and an oxide composition of $^{18}O/^{16}O$ of 0.00205 was used (Nier, 1950). Data reduction was performed using the programs Tripoli and U-Pb Redux (Bowring et al., 2011; McLean et al., 2011) and the decay constants of Jaffey et al. (1971). All Pb_c was attributed to laboratory blank with a mean isotopic composition determined by total procedural blank measurements (see Supplementary Table S1 for values). Analytical uncertainties (±X) in U-Pb zircon dates are reported in the manuscript at the 95% confidence level; 2σ uncertainties including tracer calibration (±Y) and decay constant uncertainties (±Z) are reported in Table 1. Correction for initial ^{230}Th disequilibrium in the $^{206}Pb/^{238}U$ system was made on a fraction-by-fraction basis by estimating $(Th/U)_{magma}$ using $(Th/U)_{zircon}$ determined by TIMS and a mean $(Th/U)_{zircon\text{-}magma}$ partition coefficient ratio of 0.19 ± 0.11, which encompasses the range of values for $(Th/U)_{zircon\text{-}magma}$ partition coefficients obtained from glasses from a variety of volcanic settings (Claiborne et al., 2018). Uncertainties for the resulting $(Th/U)_{magma}$ were also calculated on a fraction-by-fraction basis, propagating the uncertainty in the $(Th/U)_{zircon\text{-}magma}$ partition coefficient. U-Pb data from each analysis is provided in Supplementary Table S1.

4. Results

4.1. Sample descriptions

Outcrop photos of each sample are shown in Fig. 2, and zircon images are displayed in Fig. S1. Only the zircons that were successfully

Table 1
Alternate age interpretations. We compare our preferred eruptive age interpretation with other common ways to address complex zircon populations. All interpretations are internally consistent with little difference in age, showing that our selected interpretation will not affect the conclusions in this paper.

	Youngest zircon					Weighted means												Bayesian eruptive age with bootstrapped prior	
						Youngest few zircons							Maximum n allowed for MSWD ≈ 1						
Sample	Zircon	Age (Ma)	Uncertainty			Additional zircons	n	Age (Ma)	Uncertainty			MS WD	Additional zircons	n	Age (Ma)	Uncertainty		MS WD	Age (Ma)	Uncertainty
			X	Y	Z				X	Y	Z					X	Y	Z		
CCT18–306	z13	22.230	0.094	0.095	0.098	31,42	3	22.246	0.054	0.055	0.060	0.73	all but 2,8,18,45	17	22.320	0.016	0.021	0.032	1.0	22.302	0.040
CCT15–311	z32	20.857	0.050	0.052	0.057	31,10	3	20.863	0.024	0.027	0.035	0.043	5,9	5	20.868	0.023	0.027	0.035	0.44	20.857	0.034
CCT18–315	z35	20.572	0.040	0.043	0.048	9,15	3	20.590	0.029	0.035	0.041	0.86	25,38,40,43	7	20.609	0.022	0.028	0.036	1.1	20.575	0.040
CCT18–322	z8	20.124	0.053	0.056	0.060	9,30	3	20.142	0.030	0.033	0.040	0.37	all but 15,20,29,31	16	20.176	0.011	0.016	0.027	1.0	20.158	0.028
																				preferred interpretation	

dated are included in Fig. S1; zircons not pictured were lost at some stage of zircon chemistry prior to dating or were dated and exhibited a ratio of radiogenic Pb to common Pb that was ≤1, leading to exclusion from further analysis.

Sample CCT18-306 was collected from section height 306.7 m, from the "Livello Raffaello." With a thickness up to 40 cm, the Livello Raffaello is a regional marker bed in the Umbria-Marche basin because it is the first volcaniclastic horizon in the Miocene, found just above the contact with the underlying Scaglia Cinerea Formation. (Guerrera et al., 2015; Montanari et al., 1997; Montanari et al., 1991, 1994; Odin et al., 1991). At the CT section, the sample consists of 18 cm of bentonite, and it is thicker and more lithified than the other samples collected in this study; some excavation of a thin layer of recent cover was required to collect the sample. Zircons separated were ~ 100 μm in length, euhedral, blocky, and prismatic, with pronounced terminations.

Sample CCT15-311 was collected from a stratigraphic height of 311.3 m, from a horizon also referred to as "CT-WAL" (Montanari et al., 1997). This volcaniclastic horizon is 15 cm thick and is noted for the presence of macroscopic biotite. This sample, as well as the following two volcaniclastic samples, is recessed from the outcrop relative to the more resistant limestones on other side. Zircons extracted from this sample were mostly euhedral and prismatic, and ranged in morphology from small (<100 μm) and equant to ~500 μm and blocky, with a few thin grains. No correlation was observed between rounder zircon grains and older analyses.

Sample CCT18-315 was collected at height 315 m and is ~10 cm thick. This volcaniclastic horizon was light orange in color. Zircons dated from this sample were 50–100 μm in length, mostly euhedral and prismatic, with pronounced terminations.

Sample CCT18-322 was collected at height 322.2 m and is 40 cm thick. This volcaniclastic horizon was not well lithified and exhibited discontinuous streaks of orange. It is the last volcaniclastic layer in the CT section, just 50 cm below the end of the outcrop. Zircons separated from this sample were mostly euhedral, blocky, and 50–100 μm in length.

4.2. Sample ages

Individual zircon $^{206}Pb/^{238}U$ dates from these four samples are shown in Fig. 3, with 95% confidence intervals, and Concordia plots for each sample are found in Fig. 4; most analyses overlap with the Concordia line, consistent with closed-system behavior. A small number of grains were inherited and/or discordant; these are depicted in Fig. 4 and described in the Supplementary Table S1 but are omitted from Fig. 3 and our age models. Within each sample, dates spread beyond analytical uncertainty, most likely as a result of prolonged crystallization in the source magma, or inheritance of older grains from the volcanic edifice or host rock (Cooper, 2015; Stelten et al., 2015). For this reason, in Fig. 3 we use arrows to point out the youngest and most precise age as one estimate for the age of each volcaniclastic horizon and highlight these analyses in Fig. 4. As an alternative approach to calculating eruptive ages from disperse datasets, zircon dates and uncertainties from each sample were incorporated into a Bayesian Monte Carlo Markov Chain (MCMC) model, which makes a probabilistic estimate of eruption age based on the dated population of grains from each sample (Keller et al., 2018). Since this approach eliminates subjectivity by factoring in all zircon dates, we star and label these eruptive ages in Fig. 3 and use these ages as our preferred interpretation for the age of each volcaniclastic horizon. However, we compare this interpretation to alternative approaches in Table 1, using youngest zircon or weighted mean ages, and we find that each interpretation produces overlapping ages. Thus, our chosen eruptive age interpretation does not affect the conclusions of this paper. Full U-Pb data is found in Supplementary Table S1.

We find that the Rafaello bed, sampled in CCT18–306, is aged 22.302 ± 0.040 Ma, compared to an inverse isochron age of 21.88 ± 0.32 Ma obtained through stepwise-heating incremental release

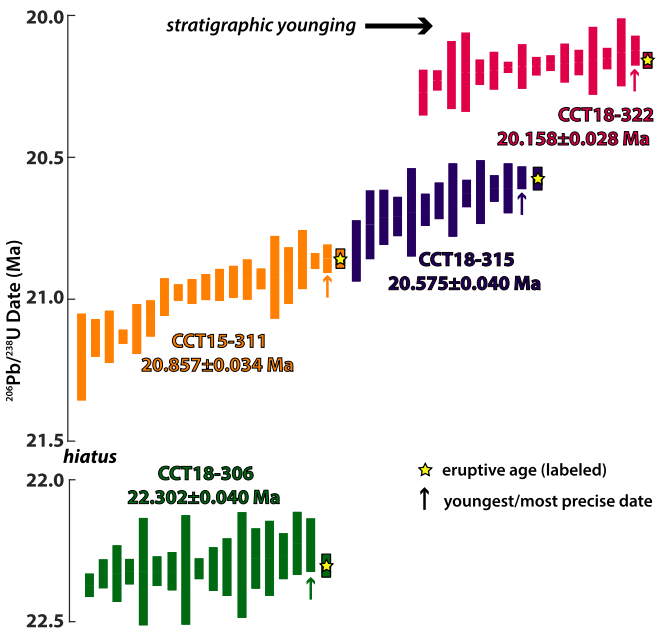

Fig. 3. Rank order plots. $^{206}Pb/^{238}U$ dates from each geochronology sample are plotted here, with stratigraphic younging of the younger three samples from left to right. Arrows indicate the youngest and most precise single analysis, and stars and labels show Bayesian eruptive ages calculated from each sample, which we highlight as our preferred interpretation. These eruptive ages are calculated from the individual zircon dates plotted here; discordant and inherited grains were excluded from these calculations.

$^{40}Ar/^{39}Ar$ geochronology on plagioclase separates by Montanari et al. (1997), using a Fish Canyon sanidine standard age of 27.84 Ma (Cebula et al., 1986). This age can be recalculated to 22.16 ± 0.32 Ma with an updated Fish Canyon sanidine age of 28.201 Ma (Kuiper et al., 2008). Next, CCT15–311 is found to be 20.857 ± 0.034 Ma, compared to the age of 19.61 ± 0.18 Ma formerly obtained for this horizon (Montanari et al., 1997), recalculated to 19.86 ± 0.18 Ma (Kuiper et al., 2008). Our age for CCT15-315 is 20.575 ± 0.040 Ma, and our age for CCT15-322, at the top of the CT section, is 20.178 ± 0.020 Ma.

5. Discussion

5.1. Zircon geochronology provides a new age model for the Miocene Contessa section

Based on the appearance of both rock samples and zircons, we agree with previous interpretations that deposition of Bisciaro Formation volcaniclastics in the CT section represents primary ash fall (e.g., Guerrera et al., 2015; Montanari et al., 1994, and references therein). To complement their analysis of the mineralogy of the bentonites, which showed 50–75% volcaniclastic supply with a low ratio of reworked to primary grains, we present evidence based on zircon geochronology. The zircons obtained from all four dated volcaniclastic horizons are mostly euhedral and prismatic, consistent with magmatic textures (Fig. S1), though cathodoluminescence images, which would bolster this interpretation for zircon origin, were not obtained due to low radiogenic Pb content of the zircons. Individual zircon ages for each of our samples are distributed over 150–900 kyr (excluding inherited grains), consistent with crystallization timescales observed in other ashes (e.g., Cooper, 2015; Kasbohm and Schoene, 2018). Our ages reflect stratigraphic order, younging in a clearly resolvable manner from the bottom to the top of the section (Fig. 3).

Given the internal consistency of our U-Pb ages, we suggest that they can be used to construct a new age model for the CT section. Our ages suggest that biostratigraphy and magnetostratigraphy previously

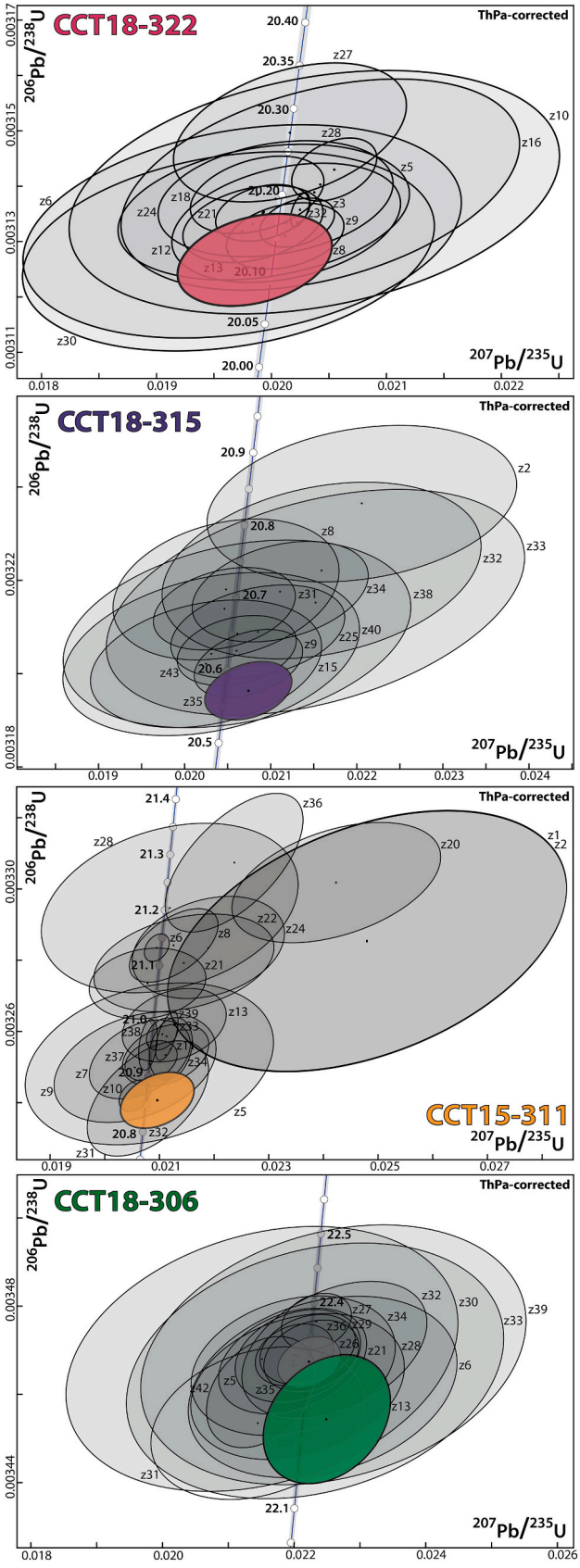

Fig. 4. Concordia plots. Concordia plots from each sample are shown here, with the youngest and most precise analyses highlighted and labeled. Multiple age interpretations for each sample are found in Table 1. Intersection with the Concordia line suggests that the zircons crystallized in a closed system.

obtained in the CT section (Montanari et al., 1997) overestimate the amount of time represented in the section (Fig. 5). Rather than being deposited between 22 and 17 Ma, deposition occurred between ~22.3 and 20.2 Ma. We suggest that the offset in U-Pb and $^{40}Ar/^{39}Ar$ ages for CCT15-315 may arise from alteration of plagioclase crystals, which was recognized as a concern following scattered ages from single crystal analyses (Montanari et al., 1991). With ~1.4 Myr elapsed between CCT18-306 and CCT15-311, our geochronology supports the biostratigraphic evidence for a substantial hiatus of ~1 Myr between these samples (Montanari et al., 1997). While a slower sedimentation rate (~3.5 m/Myr) between 306 and 311 m in the section is another possible explanation, the depositional rate would have to be five times slower than it is in the upper portion of the section (~15 m/Myr) to accommodate our ages. In addition to this inferred hiatus, we suggest that frequency of volcanic eruptions was lower between these samples than higher in the section. Prolonged zircon residence time in a magma chamber prior to the deposition of CCT15–311 would account for the greater age dispersion of zircons in this sample (over 900 kyr) than the more uniform distributions of our other geochronology samples, which were deposited at more regular intervals.

We find that nearly all of the inconsistencies between our zircon ages and the prior bio-magnetostratigraphic calibration of the section can be explained by underestimated foraminiferal stratigraphic ranges and unreliable paleomagnetic data (Fig. 5). While foraminiferal abundance and preservation in the Bisciaro Formation ranges from moderately good to very poor, at the CT section, foraminiferal preservation was poor due to recrystallization and deformation (Montanari et al., 1997). This may have led to an underestimation of the true stratigraphic range of the foraminifera; in some cases, the first occurrences in the CT section follows the regional first appearance, and the last occurrences predate their expected last appearance. For the most part, each biostratigraphic datum between our first and last geochronology samples either fits this pattern of underestimated range or falls where expected.

We can evaluate biostratigraphic data in the Contessa section observed below our first geochronology sample, CCT18-306 at ~22.3 Ma. At 301.5 m in the correlated CQ portion of the composite section, the first occurrences of *G. dehiscens*, *T. immaturus*, and *G. subquadratus* are documented together (Montanari et al., 1997), even though these events are estimated to occur at three different times (22.5 Ma (Raffi et al., 2020), 23.73 Ma (Spezzaferri et al., 2018), and 21.09 Ma (Lirer et al., 2019), respectively). While the first two events fall before our first dated sample, as expected, the third occurs prior to its anticipated first occurrence. Given the juxtaposition of these ages, this portion of the section may be subject to reworking (particularly in the case of *G. subquadratus*), underestimated stratigraphic range (for *T. immaturus*), or a hiatus. The first occurrence of *D. druggi* occurs at 305 m in the CT section (Montanari et al., 1997). This calcareous nannofossil datum is known to be diachronous and unreliable, with ages of 22.68 Ma or 22.32 Ma (Raffi et al., 2020); either is concordant with our geochronology.

A number of foraminiferal boundaries are reported between CCT18-306 and CCT15-315, (~22.3–20.8 Ma). The last occurrence of *P. kugleri* in the CT section at 307.4 m, is expected to occur at 21.09 Ma in the Mediterranean domain (at the end of Chron C6AA), based on sedimentation rate estimates from the Aquitanian GSSP section at Carrosio-Lemme, Italy (Lirer et al., 2019). In the equatorial Atlantic, in the calibrated cores from the Ceara Rise, the age of this datum is estimated to be 21.12 Ma (Raffi et al., 2020); either estimate for the top of *P. kugleri* is consistent with our eruptive ages. Next, at 309.6 m, the first occurrences of *T. trilobus* and *G. altiaperturus* are documented. In the Mediterranean domain, *T. trilobus* is expected to first appear at 22.8 Ma (Lirer et al., 2019), or at 22.96 Ma at the Ceara Rise (Raffi et al., 2020), indicating underestimated stratigraphic range for *T. trilobus*. The first occurrence of *G. altiaperturus* is expected at 21.4 Ma in the Mediterranean (Lirer et al., 2019), consistent with our geochronology. While a hiatus was inferred based on the juxtaposition of these first occurrences (Montanari et al.,

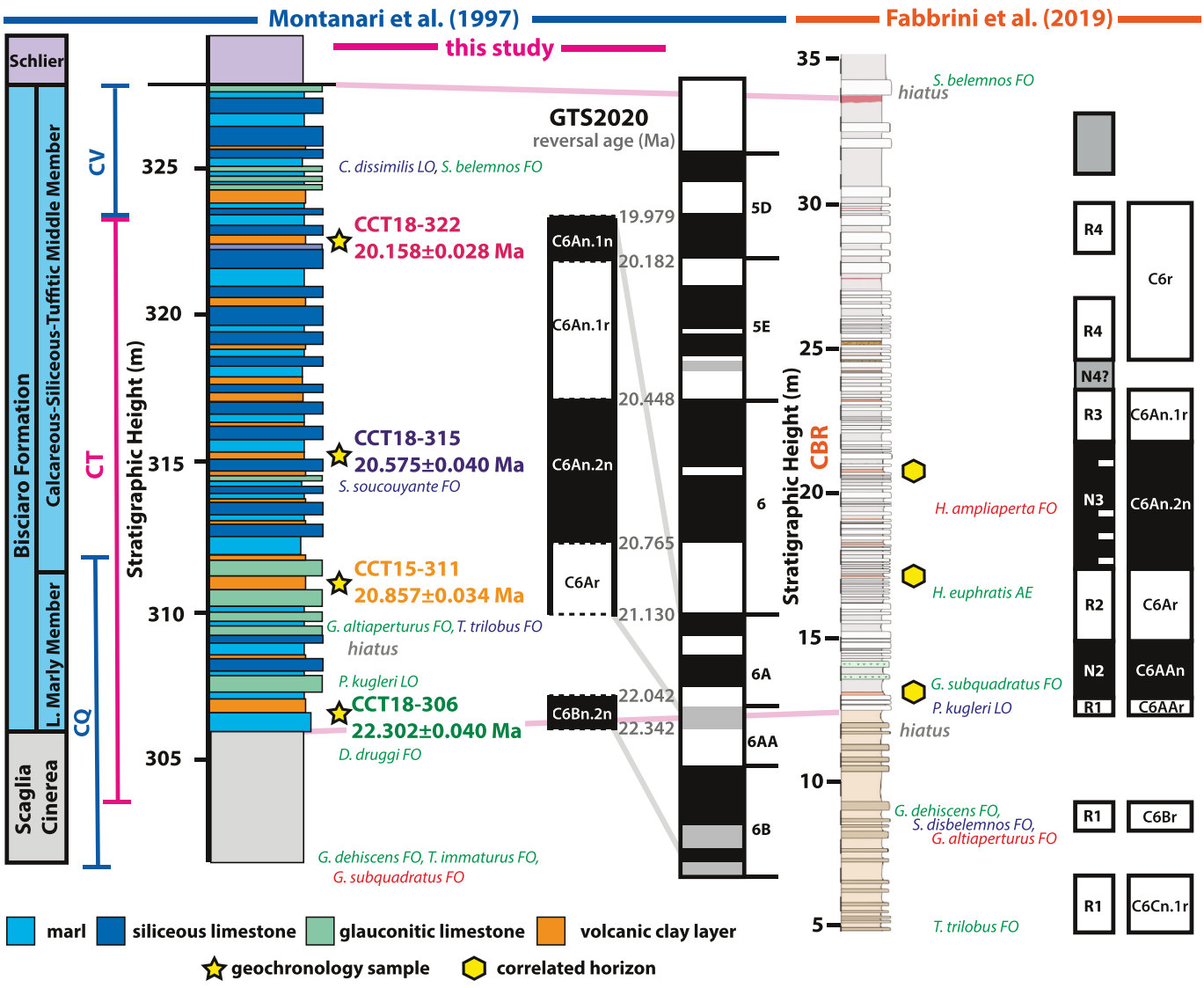

Fig. 5. Summary of Contessa section stratigraphic data. The stratigraphic section, paleomagnetic, and biostratigraphic data of Montanari et al. (1997) alongside our geochronology results for the CT section may be correlated (light pink lines) to the stratigraphic data from the CBR section of Fabbrini et al. (2019). Our ages may be correlated to the Geomagnetic Polarity Timescale presented in Raffi et al. (2020); dotted lines indicate that the stratigraphic position of magnetic field reversals in the section are unknown, although chrons C6Ar–C6An.1n are contiguous as shown. Polarity chrons inferred based on geochronology match the polarity of samples obtained at each height, though this may be accidental. Biostratigraphic data are color coded in the following manner: green when consistent with our geochronology, blue when consistent with underestimated stratigraphic range, and red when inconsistent with both geochronology and underestimated range. (For interpretation of the references to color in this figure legend, the reader is referred to the web version of this article.)

1997) and is likely given the low apparent sedimentation rate between our geochronology samples, poor preservation at lower heights in the section or sedimentary reworking may also be to blame for the underestimated range of *T. trilobus*. Underestimated stratigraphic range may also account for the first occurrence of dinoflagellate cyst *S. soucouyantae* at 314 m (~20.6 Ma in our age model), when this first occurrence is estimated to occur at 22 Ma (Hilgen et al., 2012).

The paleomagnetic data obtained by Montanari et al. (1997) documented numerous magnetic field reversals, leading to the suggestion that magnetic polarity Chrons C6B through C5D were present in the CT and overlying CV sections (~22.5–17.5 Ma). By contrast, our U-Pb ages from the CT section fall during Chrons C6Bn.2n through C6An.1n (~22.3–20.2 Ma), when compared to GTS 2020 (Raffi et al., 2020). For the most part, the magnetic polarity obtained at the stratigraphic position of each geochronology sample matches the polarity inferred from GTS 2020 (Fig. 5), though this may be accidental, as the paleomagnetic data overestimates the number of magnetic field reversals present in the section. While Montanari et al. (1997) document 14 different polarity intervals between samples CCT15-311 and CCT18-322, GTS2020 suggests that only 4 polarity chrons should be represented.

The unreliability of the paleomagnetic data in Montanari et al. (1997) may be the result of numerous factors. The magnetic mineralogy of the carbonates sampled was found to be multi-domain magnetite, which is recognized as an unreliable paleomagnetic recorder (Butler, 1992). Alternatively, the elevation of the outcrop may have made the section susceptible to a lightning-induced viscous remagnetization. Thermal demagnetization above 350 °C reportedly led to erratic behavior, far lower than the 550–580 °C unblocking temperatures of reliable paleomagnetic data recorded by single-domain magnetite. Rather than vector fitting of demagnetization directions through principal component analysis (Kirschvink, 1980), orthogonal projection diagrams were only visually inspected. Beyond these weaknesses with the data obtained, Montanari et al. (1997) also suggest that anomalous directions may arise because of delayed remanence acquisition during

lithification, bioturbation, and slow sedimentation rates of 2 m/Ma, based on $^{40}Ar/^{39}Ar$ geochronology; weathering and tectonic activity, such as faulting, may have also affected the magnetic signal.

The large number of magnetic field reversals obtained from the prior paleomagnetic data, $^{40}Ar/^{39}Ar$ geochronology, and the last occurrence of *C. dissimilis* at 325 m (in the CV portion of the section, which is across the highway but inferred as conformable with the top of CT), led to the inference of Montanari et al. (1997) that the top of the CT-CV section extended to ~17 Ma. However, our age for the top of the CT section, within 30 cm of the end of the outcrop, is 20.178 ± 0.020 Ma. While we were unable to obtain geochronology samples from the CV section due to inaccessibility, we suggest that it may face the same obstacles of calibration as the CT section. The stratigraphic range of *C. dissimilis* may also be underestimated; its last occurrence may precede the Mediterranean record of this event at 17.03 Ma, based on astronomical tuning (Lirer et al., 2019) (alternatively documented at 17.54 Ma at the Ceara Rise (Raffi et al., 2020)). This hypothesis is supported by the fact that the last occurrence of *C. dissimilis* occurs at the same stratigraphic height as the first occurrence of calcareous nannofossil *S. belemnos*, which is estimated to occur at 19.01 Ma (Backman et al., 2012). The number of magnetic field reversals observed in the uppermost portion of the section may also be either overestimated or miscorrelated. Alternatively, sedimentation rates may have slowed significantly, or there may be a depositional hiatus between the CT and CV sections.

Our work shows the importance of obtaining reliable age constraints on sedimentary records, from which major events in Earth's climate history are inferred. Unfortunately, carbonate rocks do not always yield reliable paleomagnetic records, and may be easily altered through diagenesis, tectonics, dissolution, or other processes that lead to poor foraminiferal preservation. The presence of hiatuses in the CT section complicates assessments of biostratigraphic data and the assignment of reversal signatures to polarity chrons, and inhibits the application of astronomical tuning. High-precision geochronology not only reveals these stratigraphic issues, but also provides a new age model for the section, which can be used to re-calibrate the results of prior and future studies of the Bisciaro Formation at the Contessa section. Even the latest GTS 2020 relies on the prior integrated stratigraphy from the CT section for some of its age assignments for planktonic foraminifera. In the case of the first occurrence of *G. altiaperturus*, the age of 19.97 Ma selected in GTS 2020 is based on the assignment of this datum by Montanari et al. (1991) to the base of C6r (Raffi et al., 2020), which we show in this study to be incorrect. Instead, our new CT age model indicates an age of at least 20.9 Ma, if not older, given a likely hiatus in this portion of the section. The age of 21.4 Ma for this datum proposed by Lirer et al. (2019), estimated from sedimentation rates at the Carrosio-Lemme GSSP, yields a more concurrent result with our geochronology. Thus, our new age model for the CT section contributes an improved understanding of the actual timing of this occurrence and should inform future revisions of the GTS.

5.2. The Contessa section is not a suitable candidate for the Burdigalian GSSP

A recent integrated stratigraphic study of another nearby exposure of the Miocene Contessa section, which we will refer to as the Cementerie Barbetti Quarry (CBR) section (43.38369°N, 12.56131°E, 628 m) after Coccioni et al. (2008), was put forward as a candidate for the Aquitanian-Burdigalian GSSP (Global Stratotype Section and Point) by Fabbrini et al. (2019). This section yielded a first occurrence of calcareous nannofossil *Helicosphera ampliaperta*, which is one datum suggested for the Aquitanian-Burdigalian boundary; is accessible along the road to the quarry; and in the opinion of Fabbrini et al., produced concordant planktonic foraminifera, calcareous nannofossil, and paleomagnetic data from a well-preserved outcrop. The first occurrence of *H. ampliaperta* is the favored criterion for the GSSP because it is both found in the historical stratotype for the Burdigalian and age-calibrated to 20.44 Ma in the Ceara Rise reference section (Raffi et al., 2020).

The Neogene working group seeks to locate the Burdigalian GSSP in an astronomically-tuned deep marine section in the Mediterranean, for consistency with the other Miocene GSSPs, but has thus far failed to find a suitable section (Raffi et al., 2020). Given its 200 m distance from the CT-CV section, we suggest that the new CBR section may be subject to some of the same concerns regarding imperfect paleomagnetic data, hiatuses, and underestimated biostratigraphic ranges, and thus would not be suitable for a GSSP. Although principal component analysis was performed on the paleomagnetic data, and samples taken from the same horizon gave similar directions whether subject to thermal or alternating field demagnetization, the data is still not optimal quality. Directional data with maximum angular deviation (MAD) >11° was presented as "Group B" quality data, even though samples that show this level of uncertainty are typically excluded from paleomagnetic studies. They are included here because they are bracketed by directions with lower MADs. Additionally, the *k* values of the mean directions are less than 10, indicating that the data included do not cluster well. The mean directions for each polarity group fail a reversal test, and one sampling horizon yielded both normal and reversed directions (Fabbrini et al., 2019). Despite these uncertainties, the polarity timescale for the section also suggests a hiatus between Chrons C6Br and C6AAn, which agrees with our radiometric constraints on the hiatus between CCT18–306 and CCT15–311. The presence of one or more hiatuses violates the criteria for a GSSP that sedimentation should be continuous through the section (Remane et al., 1996).

Since CBR and CT are only 200 m apart, and both exhibit 21–22 m of section between the first volcaniclastic layer and the boundary between the Bisciaro and Schlier formations, we tentatively suggest correlations between our samples CCT18-306 (the Livello Raffaello), CCT15–311, and CCT18–315, and the volcaniclastic layers at 13 m, 17 m, and 21 m at CBR (Fig. 5). It is unclear why Fabbrini et al. (2019) labeled the horizon at 14.5 m as the Livello Raffaello, without any further description of its lithology contrasting it with the other volcaniclastic layers in the section. The Livello Raffaello is recognized as the first Miocene volcaniclastic ash above the Scaglia Cinerea (Guerrera et al., 2015; Montanari et al., 1994), and so we suggest correlating CCT18-306 with the horizon at 13 m in CBR is more consistent with this definition, and furthermore allows for improved correlations and similar sedimentation rates between these two sections. Alternatively, it could be argued that the Livello Raffaello should be correlated as labeled in CBR, and CCT15-311 and CCT18-315 should be aligned with the biotite-bearing horizons at 16.25 m and 19 m in CBR. However, this would lead to a non-linear sedimentation rate within CBR, significantly slower sedimentation rates at CBR than at CT, and a greater degree of biostratigraphic inaccuracy. We therefore suggest the correlation between sections shown in Fig. 5.

While the foraminiferal preservation in CBR is described as generally moderate, there are also intervals of poor preservation, particularly near the volcaniclastic horizons (Fabbrini et al., 2019). We can first evaluate the biostratigraphic data in proximity to the Livello Raffaello volcaniclastic horizon at 13 m, correlated to our age for CCT18-306 of ~22.3 Ma. The first occurrence of *T. trilobus*, expected at 22.8 Ma in the Mediterranean (Lirer et al., 2019), is found at 4.7 m, consistent with our geochronology and with the magnetochron assignment of C6Cn.1r (Raffi et al., 2020). Next, first occurrences for *G. dehiscens*, *S. disbelemnos*, and *G. altiaperturus* are found at 7.8 m, with expected ages of 22.5 Ma, 22.9 Ma, and 21.4 Ma, respectively (Lirer et al., 2019; Raffi et al., 2020). While *G. altiapterurus* falls out of order relative to the age of the Livello Raffaello, the other data are younger than 22.3 Ma, as expected. However, the first occurrence of *S. disbelemnos* is recorded at 22.9 Ma in upper Chron C6Cn.1r, while at CBR it falls during Chron C6Br, indicating underestimated stratigraphic range for this datum.

The last occurrence of *P. kugleri* is observed just below the volcaniclastic layer at 13 m (Fabbrini et al., 2019), which is in disagreement with the CT section, where it is found 70 cm above CCT-306 (Montanari

et al., 1997). This inconsistency could be explained in two possible ways. First, the last occurrence at CBR may precede the Mediterranean last occurrence at 21.09 Ma (Lirer et al., 2019) with underestimated stratigraphic range. At CBR, *P. kugleri* is described as rare, especially near the base and top of its occurrence, smaller in size, and hardly detectable, which lends support for this possibility. Alternatively, the Livello Raffaello may represent a diachronous horizon, despite its designation as a regional marker bed, though this possibility seems unlikely given the close proximity between CT and CBR. Without a detailed interrogation of its accuracy, the biostratigraphic data from CBR is used to infer that the hiatus between Chrons C6Br and C6AAn occurs prior to Livello Raffaello deposition, whereas our data suggests it occurs afterwards. The last occurrence of *P. kugleri* is also used to suggest that the Livello Raffaello is 21.09–21.08 Ma (Fabbrini et al., 2019), which is inconsistent with our eruptive age for this horizon. If the layers are the same age (which could be tested with zircon geochronology at CBR), we suggest that the biostratigraphic age calibration of CBR may be erroneous, at least in the vicinity of the *P. kugleri* last occurrence.

Though *G. subquadratus* was found out of stratigraphic order at CT, prior to its expected first occurrence at 21.4 Ma (Lirer et al., 2019), it falls just above the Livello Raffaello at CBR (Fabbrini et al., 2019), concordant with our age for CCT18-306. The acme end of *H. euphratis* is found just below the horizon correlated with CCT15-311, and the estimated age of this event at 20.98 Ma (Raffi et al., 2020) concurs with our age of 20.857 ± 0.034 Ma. But the critical, potentially GSSP-defining first occurrence of *H. ampliaperta*, estimated at 20.43 Ma (Raffi et al., 2020), falls between horizons correlated to CCT15–311 and CCT18–315 (20.575 ± 0.040 Ma), suggesting that this occurrence at CBR is premature. While the reliability of the first occurrence of *H. ampliaperta* is indistinct in terms of abundance change, it is recognized as isochronous within 20–100 kyr (Raffi et al., 2020). Its location in CBR indicates that this datum is either less isochronous than previously thought, or the result of reworking at CBR. Reworking appears to be a distinct possibility as this datum is interpreted by Fabbrini et al. (2019) to occur during Chron C6An.2n, whereas an age of 20.43 Ma would place this occurrence in the following polarity Chron, C6An.1r (Raffi et al., 2020).

Due to the biostratigraphic inconsistencies with our radiometric age model, paleomagnetic data that is not of the highest statistical quality, and the presence of three major hiatuses in the section, we suggest that the CBR section not be adopted as a GSSP. Furthermore, selecting this section on the basis of its first occurrence of *Helicosphera ampliaperta* should also be questioned, since this datum likely occurs out of order at CBR. Also, while this nannofossil is a reliable marker in the Mediterranean, it is not common in the open ocean (Raffi et al., 2020), and thus cannot be broadly applied to locate the Aquitanian-Burdigalian boundary in the ocean drill core record. Alternative placements for the Burdigalian GSSP include the last appearance of *P. kugleri* at 21.12 Ma, the top of magnetic polarity Chron C6An at 19.979, or the first occurrence of *S. belemnos* at 19.01 Ma (Raffi et al., 2020). However, at CBR the range of *P. kugleri* is likely underestimated, the inferred position of the top of C6An is poorly constrained by paleomagnetic data, and the first occurrence of *S. belemnos* is adjacent to an inferred hiatus (Fabbrini et al., 2019), so CBR does not yield a fitting GSSP by these criteria either.

Recently, it has been suggested that the “golden spike” of GSSPs be located in ash beds amenable to dating through high-precision U-Pb zircon geochronology, since the ages of ashes can be determined with greater precision than biostratigraphic data (Davydov, 2020). While our new geochronology yields ages for ashes in the CT section, the issues with bio- and magnetostratigraphic correlation that we enumerate here show that neither CT nor CBR would be good candidates for the Burdigalian GSSP. Due to the difficulty in finding terrestrial exposures at the base of the Burdigalian amenable to orbital tuning, magnetostratigraphy, and micropaleontological analysis, there has been ongoing discussion of placing the Burdigalian GSSP in a well-described ocean drill core (Ogg et al., 2016; Raffi et al., 2020), which would ideally avoid the stratigraphic issues in CBR that we have detailed here.

The comparison of CBR and CT shows the importance of obtaining high-precision geochronology as a necessary corroboration of biostratigraphic and magnetostratigraphic age calibration, especially for sections treated as possible GSSPs. Interpreting recent research from the very stratigraphic section we studied proves this point. In a study of the Miocene Mediterranean Sr and Nd isotopic record, Cornacchia et al. (2018) collected samples from the CT section that were calibrated in age based on $^{40}Ar/^{39}Ar$ geochronology from Montanari et al. (1997). One sample, two meters above the Livello Raffaello, with an estimated age of 21.1 Ma and elevated $^{87}Sr/^{86}Sr$ levels is suggested to be coeval with the Mi-1a event, reflecting increased continental runoff as a result of greater weathering during a transient glaciation (Cornacchia et al., 2018). The age model from CBR based on bio- and magnetostratigraphy suggests that this event would postdate their estimated age of 21.09 Ma for the Livello Raffaello, leading Fabbrini et al. (2019) to reject the correlation with the Mi-1a event. By contrast, an age of 21.1 Ma concurs with our radiometric age model, bounded by two high-precision eruptive ages, and furthermore, our age model could be used to refine the age estimates of the other CT samples presented in Cornacchia et al. (2018).

5.3. Geochronology may help constrain the provenance of the Bisciaro volcaniclastics

Petrography of the volcaniclastic layers of the Bisciaro Formation have led to a debate on the source of these layers. Western Sardinia has been the leading candidate as the source of explosive volcanism that produced the Bisciaro ashfall. Montanari et al. (1994) performed a grain size analysis of the felsic fraction of the Livello Raffaello, and found that grain size decreased from southwest to northeast through the Umbria-Marche basin, consistent with ash carried by westerly winds from Sardinia. Assorgia et al. (1994) analyzed biotites present in the volcaniclastic units of the Bisciaro and Schlier Formations, and found that their geochemistry matched that of the calc-alkaline volcanic sequence at Bosa, on the west coast of Sardinia. While $^{40}Ar/^{39}Ar$ geochronology has been used to estimate the main phase of early Miocene volcanism on Sardinia to occur between 20.5 and 18 Ma (Gattacceca et al., 2007), this hypothesis could be further tested by performing zircon geochronology on volcanic units in Sardinia, to see if any particular eruptions match our eruptive ages from the CT section. If these argon data are correct and complete, an alternative source of felsic volcanism may be required to explain the presence of the Livello Raffaello, which we have dated to 22.3 Ma.

By contrast, Guerrera et al. (2015) argue that while Sardinian volcanism may be responsible for fine-grained volcaniclastic pelites in the Bisciaro Formation, it would be too distant to produce the turbiditic volcaniclastic horizons observed elsewhere in the Bisciaro. Instead, they infer a more proximal source of volcanism, from the subduction of the Mesomediterranean microplate under Adria. However, there are no volcanic edifices preserved from this event, potentially as a result of rapid erosion, subsidence, or burial by underthursting (Guerrera et al., 2015). Future high-precision geochronological studies in the Mediterranean could assist with identifying the provenance of the Bisciaro volcaniclastics and correlating them with other early Miocene volcaniclastic deposits around the Mediterranean (listed in Guerrera et al., 2015).

6. Conclusions

Our work shows the importance of absolute radioisotopic calibration of carbonate sucessions to allow for more accurate determinations of the timing and tempo of Earth system changes. Our new high-precision U-Pb geochronology from Lower Miocene carbonates in the Contessa Valley, Italy, a noted archive of Cretaceous to Middle Miocene Earth history, ground-truths the prior temporal calibration for these sediments that had been provided by legacy $^{40}Ar/^{39}Ar$ geochronology, biostratigraphy, and magnetostratigraphy. Our new eruptive ages from four

volcaniclastic horizons show that this section was deposited between ~22.3 and 20.1 Ma, with a hiatus lasting ~1 Ma in the Lower Bisciaro, in contrast to the prior age model that suggested deposition between ~22 and 17 Ma. By providing a new radiometric age model for the CT section, we show that Miocene sections in the Contessa Valley would not serve as a suitable GSSP for the Aquitanian-Burdigalian boundary and suggest that alternatives be pursued. Our work also may contribute to an improved understanding of the provenance of the Bisciaro volcaniclastics. In stratigraphic sections with zircon-bearing volcanic ashbeds, radioisotopic numerical ages can and should be used as a necessary backbone for calibrating the Geologic Timescale, to ensure the proper alignment of critical records of Earth's environmental history.

Declaration of Competing Interest

The authors declare that they have no known competing financial interests or personal relationships that could have appeared to influence the work reported in this paper.

Acknowledgements

D. Santiago-Ramos assisted in the field campaign, C. Chiodo helped with field logistics, and L. O'Connor assisted with zircon separation. H. Li, an anonymous reviwer, and editor T. Algeo provided constructive feedback on earlier versions of this manuscript. We also thank the Association “Le Montagne di San Francesco” for logistical support during field work. Funding for this project was provided by Princeton University Department of Geosciences through the Geosciences Student Research Fund and by the Scott Vertebrate Fund.

Appendix A. Supplementary data

Supplementary data to this article can be found online at https://doi.org/10.1016/j.palaeo.2021.110487.

References

Alvarez, W., 2019. A review of the Earth history record in the Cretaceous, Paleogene, and Neogene pelagic carbonates of the Umbria-Marche Apennines (Italy): twenty-five years of the Geological Observatory of Coldigioco. Spec. Pap. Geol. Soc. Am. 542, 501–532. https://doi.org/10.1130/2019.2542(01).

Alvarez, L.W., Alvarez, W., Asaro, F., Michel, H.V., 1980. Extraterrestrial cause for the Cretaceous-Tertiary extinction. Science 208, 1095–1107. https://doi.org/10.1126/science.208.4448.1095.

Assorgia, A., Chan, L.S., Deino, A.L., Garbarino, C., Montanari, A., Rizzo, R., Tocco, S., 1994. Volcanigenic and paleomagnetic studies on the Cenozoic calc-alkalic eruptive sequence of Monte Furru (Bosa, mid-western Sardinia). G. di Geol. 56, 17–29.

Backman, J., Raffi, I., Rio, D., Fornaciari, E., Pälike, H., 2012. Biozonation and biochronology of Miocene through Pleistocene calcareous nannofossils from low and middle latitudes. Newslett. Stratigr. 45, 221–244. https://doi.org/10.1127/0078-0421/2012/0022.

Bowring, J.F., McLean, N.M., Bowring, S.A., 2011. Engineering cyber infrastructure for U-Pb geochronology: tripoli and U-Pb-Redux. Geochem. Geophys. Geosyst. 12 https://doi.org/10.1029/2010GC003479.

Butler, R.F., 1992. Paleomagnetism: magnetic domains to geologic terranes. In: Paleomagn. Magn. Domains to Geol. Terranes. https://doi.org/10.5860/choice.29-5708.

Cebula, G.T., Kunk, M.J., Mehnert, H.H., Naeser, C.W., Obradovich, J.D., Sutter, J.F., 1986. The fish Canyon Tuff, a potential standard for the $^{40}Ar/^{39}Ar$ and fission-track methods. Terra Cogn. 6, 139–140.

Claiborne, L.L., Miller, C.F., Gualda, G.A., Carley, T.L., Covey, A.K., Wooden, J.L., Fleming, M.A., 2018. Zircon as magma monitor: robust,temperature-dependent partition coefficients from glass and zircon surface and rim measurements from natural systems. In: Moser, D.E., Corfu, F., Darling, J.R., Reddy, S.M., Tait, K. (Eds.), Microstructural Geochronology: Planetary Records Down to Atom Scale, pp. 3–33.

Coccioni, R., Marsili, A., Montanari, A., Bellanca, A., Neri, R., Bice, D.M., Brinkhuis, H., Church, N., Macalady, A., McDaniel, A., Deino, A., Lirer, F., Sprovieri, M., Maiorano, P., Monechi, S., Nini, C., Nocchi, M., Pross, J., Rochette, P., Sagnotti, L., Tateo, F., Touchard, Y., Van Simaeys, S., Williams, G.L., 2008. Integrated stratigraphy of the Oligocene pelagic sequence in the Umbria-Marche basin (northeastern Apennines, Italy): a potential Global Stratotype Section and Point (GSSP) for the Rupelian/Chattian boundary. Bull. Geol. Soc. Am. 120, 487–511. https://doi.org/10.1130/B25988.1.

Coccioni, R., Frontalini, F., Bancalà, G., Fornaciari, E., Jovane, L., Sprovieri, M., 2010. The Dan-C2 hyperthermal event at Gubbio (Italy): global implications, environmental effects, and cause(s). Earth Planet. Sci. Lett. 297, 298–305. https://doi.org/10.1016/j.epsl.2010.06.031.

Condon, D.J., Schoene, B., McLean, N.M., Bowring, S.A., Parrish, R.R., 2015. Metrology and traceability of U-Pb isotope dilution geochronology (EARTHTIME Tracer Calibration Part I). Geochim. Cosmochim. Acta 164, 464–480. https://doi.org/10.1016/j.gca.2015.05.026.

Cooper, K.M., 2015. Timescales of crustal magma reservoir processes: insights from U-series crystal ages. Geol. Soc. Spec. Publ. 422, 141–174. https://doi.org/10.1144/SP422.7.

Cornacchia, I., Agostini, S., Brandano, M., 2018. Miocene oceanographic evolution based on the Sr and Nd isotope record of the Central Mediterranean. Paleoceanogr. Paleoclimatol. 33, 31–47. https://doi.org/10.1002/2017PA003198.

Davydov, V.I., 2020. Shift in the paradigm for GSSP boundary definition. Gondwana Res. 86, 266–286. https://doi.org/10.1016/j.gr.2020.06.005.

Davydov, V.I., Korn, D., Schmitz, M.D., Gradstein, F.M., Hammer, O., 2012. The carboniferous period. In: The Geologic Time Scale. Elsevier, pp. 603–651. https://doi.org/10.1016/B978-0-444-59425-9.00023-8.

Day, M.O., Ramezani, J., Bowring, S.A., Sadler, P.M., Erwin, D.H., Abdala, F., Rubidge, B. S., 2015. When and how did the terrestrial mid-Permian mass extinction occur? Evidence from the tetrapod record of the Karoo Basin, South Africa. Proc. R. Soc. B. https://doi.org/10.1098/rspb.2015.0834.

Deino, A.L., Channell, J.E.T., Coccioni, R., De Grandis, G., DePaolo, D.J., Fornaciari, E., Emmanuel, L., Laurenzi, M.A., Montanari, A., Rio, D., Renard, M., 1997. Integrated stratigraphy of the Upper Burdigalian-Lower Langhian section at Moria (Marche Region, Italy). In: Miocene Stratigraphy: An Integrated Approach, pp. 315–341.

Fabbrini, A., Baldassini, N., Caricchi, C., Foresi, L.M., Sagnotti, L., Dinarés-Turell, J., Di Stefano, A., Lirer, F., Menichetti, M., Winkler, A., Distefano, S., 2019. In search of the Burdigalian GSSP: new evidence from the Contessa Section (Italy). Ital. J. Geosci. 138, 274–295. https://doi.org/10.3301/IJG.2019.07.

Galeotti, S., Krishnan, S., Pagani, M., Lanci, L., Gaudio, A., Zachos, J.C., Monechi, S., Morelli, G., Lourens, L., 2010. Orbital chronology of early Eocene hyperthermals from the Contessa Road section, Central Italy. Earth Planet. Sci. Lett. 290, 192–200. https://doi.org/10.1016/j.epsl.2009.12.021.

Gattacceca, J., Deino, A., Rizzo, R., Jones, D.S., Henry, B., Beaudoin, B., Vadeboin, F., 2007. Miocene rotation of Sardinia: new paleomagnetic and geochronological constraints and geodynamic implications. Earth Planet. Sci. Lett. 258, 359–377. https://doi.org/10.1016/j.epsl.2007.02.003.

Gerstenberger, H., Haase, G., 1997. A highly effective emitter substance for mass spectrometric Pb isotope ratio determinations. Chem. Geol. 136, 309–312. https://doi.org/10.1016/S0009-2541(96)00033-2.

Guerrera, F., Martín-Martín, M., Raffaelli, G., Tramontana, M., 2015. The early Miocene “Bisciaro volcaniclastic event” (northern Apennines, Italy): a key study for the geodynamic evolution of the central-western Mediterranean. Int. J. Earth Sci. 104, 1083–1106. https://doi.org/10.1007/s00531-014-1131-5.

Hilgen, F.J., Lourens, L.J., Van Dam, J.A., Beu, A.G., Boyes, A.F., Cooper, R.A., Krijgsman, W., Ogg, J.G., Piller, W.E., Wilson, D.S., 2012. Chapter 29 - The Neogene Period, The Geologic Time Scale 2012 2-Volume Set. https://doi.org/10.1016/B978-0-444-59425-9.00029-9.

Jaffey, A.H., Flynn, K.F., Glendenin, L.E., Bentley, W.C., Essling, A.M., 1971. Precision measurement of half-lives and specific activities of ^{235}U and ^{238}U. Phys. Rev. C 4, 1889–1906. https://doi.org/10.1103/PhysRevC.4.1889.

Jovane, L., Florindo, F., Coccioni, R., Dinarès-Turell, J., Marsili, A., Monechi, S., Roberts, A.P., Sprovieri, M., 2007. The middle Eocene climatic optimum event in the Contessa Highway section, Umbrian Apennines, Italy. Bull. Geol. Soc. Am. 119, 413–427. https://doi.org/10.1130/B25917.1.

Jovane, L., Sprovieri, M., Coccioni, R., Florindo, F., Marsili, A., Laskar, J., 2010. Astronomical calibration of the middle Eocene Contessa Highway section (Gubbio, Italy). Earth Planet. Sci. Lett. 298, 77–88. https://doi.org/10.1016/j.epsl.2010.07.027.

Kasbohm, J.J., Schoene, B., 2018. Rapid eruption of the Columbia River flood basalt and correlation with the mid-Miocene climate optimum. Sci. Adv. 4, 1–8. https://doi.org/10.1126/sciadv.aat8223.

Keller, C.B., Schoene, B., Samperton, K.M., 2018. A stochastic sampling approach to zircon eruption age interpretation. Geochem. Perspect. Lett. 31–35. https://doi.org/10.7185/geochemlet.1826.

Kirschvink, J.L., 1980. The least-squares line and plane and the analysis of palaeomagnetic data. Geophys. J. R. Astron. Soc. 62, 699–718. https://doi.org/10.1111/j.1365-246X.1980.tb02601.x.

Krogh, T.E., 1973. A low-contamination method for hydrothermal decomposition of zircon and extraction of U and Pb for isotopic age determinations. Geochim. Cosmochim. Acta 37, 485–494. https://doi.org/10.1016/0016-7037(73)90213-5.

Kuiper, K.F., Deino, A.L., Hilgen, F.J., Krijgsman, W., Renne, P.R., Wijbrans, J.R., 2008. Synchronizing rock clocks of earth history. Science 320, 500–504. https://doi.org/10.1126/science.1154339.

Lirer, F., Foresi, L.M., Iaccarino, S.M., Salvatorini, G., Turco, E., Cosentino, C., Sierro, F. J., Caruso, A., 2019. Mediterranean Neogene planktonic foraminifer biozonation and biochronology. Earth Sci. Rev. 196, 102869. https://doi.org/10.1016/j.earscirev.2019.05.013.

Mattinson, J.M., 2005. Zircon U-Pb chemical abrasion (“CA-TIMS”) method: combined annealing and multi-step partial dissolution analysis for improved precision and accuracy of zircon ages. Chem. Geol. 220, 47–66. https://doi.org/10.1016/j.chemgeo.2005.03.011.

McLean, N.M., Bowring, J.F., Bowring, S.A., 2011. An algorithm for U-Pb isotope dilution data reduction and uncertainty propagation. Geochem. Geophys. Geosyst. 12. https://doi.org/10.1029/2010GC003478.

McLean, N.M., Condon, D.J., Schoene, B., Bowring, S.A., 2015. Evaluating uncertainties in the calibration of isotopic reference materials and multi-element isotopic tracers (EARTHTIME Tracer Calibration Part II). Geochim. Cosmochim. Acta 164, 481–501. https://doi.org/10.1016/j.gca.2015.02.040.

Montanari, A., Deino, A., Coccioni, R., Langenheim, V.E., Capo, R., Monechi, S., 1991. Geochronology, Sr isotope analysis, magnetostratigraphy, and plankton stratigraphy across the Oligocene-Miocene boundary in the Contessa section (Gubbio, Italy). Newslett. Stratigr. 23, 151–180. https://doi.org/10.1127/nos/23/1991/151.

Montanari, A., Carey, S., Coccioni, R., Deino, A., 1994. Early Miocene tephra in the Apennine pelagic sequence: an inferred Sardinian provenance and implications for western Mediterranean tectonics. Tectonics 13, 1120–1134. https://doi.org/10.1029/94TC00295.

Montanari, A., Bice, D.M., Capo, R., Coccioni, R., Deino, A.L., DePaolo, D.J., Emmanuel, L., Monechi, S., Renard, M., Zevenboom, D., 1997. Integrated stratigraphy of the Chattian to mid-Burdigalian pelagic sequence of the Contessa Valley (Gubbio, Italy). In: Montanari, A., Odin, G.S., Coccioni, R. (Eds.), Miocene Stratigraphy: An Integrated Approach. Elsevier, pp. 249–277.

Nier, A.O., 1950. A redetermination of the relative abundances of the isotopes of carbon, nitrogen, oxygen, argon, and potassium. Phys. Rev. 77, 789–793. https://doi.org/10.1103/PhysRev.77.789.

Odin, G.S., Barbin, V., Hurford, A.J., Baadsgaard, H., Galbrun, B., Gillot, P.Y., 1991. Multi-method radiometric dating of volcano-sedimentary layers from northern Italy: age and duration of the Priabonian stage. Earth Planet. Sci. Lett. 106, 151–168. https://doi.org/10.1016/0012-821X(91)90069-T.

Ogg, J.G., Ogg, G.M., Gradstein, F.M., 2016. Neogene. In: A Concise Geologic Time Scale, pp. 203–210. https://doi.org/10.1016/B978-0-444-59467-9.00015-7.

Raffi, I., Wade, B.S., Pälike, H., 2020. The neogene period. In: Gradstein, F.M., Ogg, J.G., Schmitz, M.D., Ogg, G.M. (Eds.), Geologic Time Scale 2020. Elsevier B.V., pp. 1141–1215. https://doi.org/10.1016/B978-0-12-824360-2.00029-2

Remane, J., Bassett, M.G., Cowie, J.W., Gohrbandt, K.H., Lane, H.R., Michelsen, O., Naiwen, W., 1996. Revised guidelines for the establishment of global chronostratigraphic standards by the International Commission on Stratigraphy (ICS). Episodes 19, 77–81. https://doi.org/10.18814/epiiugs/1996/v19i3/007.

Samperton, K.M., Schoene, B., Cottle, J.M., Keller, C.B., Crowley, J.L., Schmitz, M.D., 2015. Magma emplacement, differentiation and cooling in the middle crust: Integrated zircon geochronological-geochemical constraints from the Bergell Intrusion, Central Alps. Chem. Geol. 417, 322–340. https://doi.org/10.1016/j.chemgeo.2015.10.024.

Schoene, B., Guex, J., Bartolini, A., Schaltegger, U., Blackburn, T.J., 2010. Correlating the end-Triassic mass extinction and flood basalt volcanism at the 100 ka level. Geology 38, 387–390. https://doi.org/10.1130/G30683.1.

Schoene, B., Samperton, K.M., Eddy, M.P., Keller, G., Adatte, T., Bowring, S.A., Khadri, S. F.R., Gertsch, B., 2015. U-Pb geochronology of the Deccan Traps and relation to the end-cretaceous mass extinction. Science 347, 182–184. https://doi.org/10.1126/science.aaa0118.

Spezzaferri, S., Olsson, R.K., Hemleben, C., 2018. Taxonomy, biostratigraphy, and phylogeny of Oligocene to Lower Miocene globigerinoides and trilobatus. In: Wade, B.S., Olsson, R.K., Pearson, P.N., Huber, B.T., Berggren, W.A. (Eds.), Atlas of Oligocene Planktonic Foraminifera. Cushman Foundation for Foraminiferal Research, pp. 269–306.

Stelten, M.E., Cooper, K.M., Vazquez, J.A., Calvert, A.T., Glessner, J.J.G., 2015. Mechanisms and timescales of generating eruptible rhyolitic magmas at Yellowstone Caldera from Zircon and sanidine geochronology and geochemistry. J. Petrol. 56, 1607–1642. https://doi.org/10.1093/petrology/egv047.